10. PLASMA-WALL INTERACTIONS AND VACUUM QUALITY

10.1. Relevance of the Plasma Boundary Program to the QPS Mission

It has been established over the past two decades of fusion research that the control of neutrals and impurities is a prerequisite for enhanced plasma confinement. To this extent, power and particle handling has become a key element for optimizing the performance of any fusion device. Even though the control of plasma-surface interactions and the development of plasma-facing components (PFCs) are not primary objectives of QPS, they become secondary objectives in support of the QPS mission.

To achieve good plasma performance, influx of both neutrals and impurities into the core plasma should be minimized in QPS. This can be achieved through the boundary configuration and choice of materials and design of the PFCs on the one hand, and through optimized plasma operation on the other hand. It has been demonstrated in the past that reduction of recycling and impurity influx both has led to improvement of confinement in tokamaks [1, 2, 3] and stellarators [4, 5], although the question of the relative importance of neutrals vs. impurities has never been resolved.

The effect of neutrals on plasma confinement in toroidal configurations is not fully understood, but it has been shown that charge-exchange (cx) processes in the edge can cause enough momentum removal from the edge to result in friction forces comparable or larger than the effect of neoclassical damping [6, 7]. This damping of the plasma rotation by cx-friction is a possible candidate for causing limitations on plasma performance.

The impurity story in toroidal devices is complex and we are just beginning to understand some of the details. The goal of impurity control is to reduce the concentration of intrinsic impurities such as oxygen and carbon as far as possible by wall conditioning and other methods. This has dramatically improved plasma confinement as e.g. in the VH-mode [3] or Supershot-mode [8]. Subsequently, another improvement of plasma performance was achieved by seeding the plasma edge with extrinsic impurities, such as neon, which were selected to produce a particular radiation profile in the edge [9]. The result was a plasma with a radiating mantle and improved confinement. It has been shown that impurity injection reduced long wave-length turbulence in the edge which is assumed to be responsible for anomalous transport [10]. Radiating mantles might turn out to be well suited for operation in ergodic boundaries of stellarators, because radiation distributes power fluxes more uniformly to the walls than conduction and convection which could help to simplify the surface interaction of the complicated three-dimensional boundary plasma structures with limiters or divertor plates.

Overall, to accomplish the goals of the QPS program, it is clear that we need to achieve plasmas with the highest possible confinement and pressure for given machine capabilities. At

a given magnetic configuration, the control of recycling neutrals and impurities is a key ingredient towards achieving this goal.

10.2 Vacuum and Wall Conditioning

10.2.1. Vacuum Vessel and Pumping

A comparison between a vacuum vessel, more or less conformal with the plasma, and a bell jar housing the plasma, the coils and most of the other machine components, led to the decision to utilize an existing aluminum bell jar (cf. discussion in section 3.6) which had been used in the past for the ORMAK experiment [11]. This eliminates the need for building a very complex three-dimensional vacuum vessel and it simplifies many issues which are a consequence of the complex plasma and coil shape. In particular, it greatly enhances the access to the plasma for heating and diagnostics. But, on the other hand, this solution requires vacuum-tight casing of all in-vessel components.

The achievable vacuum is given by the applied pumping speed, the total leak rate and the outgassing rate of all internal surfaces. Practical pumping speeds which can be applied to QPS are typically $S = 5000\ Ls^{-1}$ at the pumps or $S_{eff} = 2500\ Ls^{-1}$ at the vacuum vessel, provided by two existing Balzers turbomolecular pumps.

Typical leak rates in today's plasma devices with all flanges, seals, etc. are $Q_L \leq 10^{-5}$ Torr-Ls^{-1}. This should be achievable in the QPS bell jar if the main seals are double-seals with differential pumping. The required base pressure prior to plasma operation in the bell jar is $p_o \leq 10^{-8}$ Torr; which would require pumping with an effective speed of $S_{eff} \geq 10^3\ Ls^{-1}$. The assumed effective pumping speed of $2500Ls^{-1}$ should be sufficient to reach the required base pressure.

Outgassing rates depend on material and treatment. With the aluminum bell jar and stainless steel casings of the coils, we will have approximately equal surface areas of aluminum and stainless steel in the vacuum vessel. The outgassing rates of aluminum have been measured to be similar to stainless steel [12]. Typical values for aluminum are 6×10^{-6} Torr-$Lm^{-2}s^{-1}$ for fresh aluminum and 4×10^{-10} Torr-$Lm^{-2}s^{-1}$ for aluminum baked at 100°C for 20 hours [12]. We see that baking can reduce the outgassing rate up to four orders of magnitude. Assuming that the residual pressure due to outgassing should not exceed the pressure caused by the leak rate, we need to aim at a total outgassing rate which is also $Q_o \leq 10^{-5}$ Torr-Ls^{-1}. The total surface area of the bell jar is approximately 75 m^2 (Al) and we allow for the in-vessel components about the same surface area, i.e. we have a total surface area of approximately 150 m^2, resulting in an allowable outgassing rate of 10^{-5} Torr-$Ls^{-1}/150m^2$, i.e. 6.6×10^{-8} Torr-$Ls^{-1}m^{-2}$. Hence, we need an outgassing rate approximately two orders of magnitude below the value of fresh aluminum, which should be achievable with mild baking. The residual outgassing for stainless steel baked for 20 hours at 100°C was measured at 1×10^{-8}Torr-$Lm^{-2}s^{-1}$ [12], well within our criterion for the maximum allowable outgassing rates.

The differentially-pumped seals (viton o-rings) in the bell jar can make up a fairly large surface area and may contribute significantly to the overall outgassing rate. The outgassing rate for viton is quoted as 4 x 10^{-3} Torr-$Lm^{-2}s^{-1}$ initially [13] and 1.8 x 10^{-3} Torr-$Lm^{-2}s^{-1}$ after 4 hours of pumping. Estimating a total surface area of 4 m^2 of exposed viton, and a pumping speed of S_{eff} = 2500 Ls^{-1}, the pressure due to the viton outgassing will be p = 2.8 x 10^{-6}Torr, clearly above the needed value. Baking viton in air for 4 hours at 150°C can reduce the outgassing rate by more than two orders of magnitude. This procedure will provide the low outgassing rates leading the required base pressure.

Previous experience using the existing bell jar in the ORMAK experiment yielded base pressures of p = 2 x 10^{-7} Torr at room temperature with 2 x 10^4 L/s pumping speed [14]; these values are consistent with the above estimates for viton outgassing. When ORMAK was cooled down to liquid nitrogen temperatures, base pressures of 10^{-8} Torr were achieved.

10.2.2. Vessel Bakeout

Unbaked metal vessels can release up to 100 monolayers (~10^{21} particles per m^2) of water molecules at elevated wall temperatures or by plasma bombardment. Baking can reduce outgassing rates by orders of magnitude, in metals as well as in graphite. The necessary temperature depends on the binding energies of the outgassing species. For metal walls, bake-out temperatures of 150-200ºC for 24 hours can reduce outgassing by 3-4 orders of magnitude, after which the base pressure is usually in the 10^{-8} Torr range, with hydrogen being the dominant residual gas. This residual hydrogen originates from the manufacturing process and can be driven out by baking at temperatures of 400ºC. This latter technique is used in UHV applications and usually results in residual pressures in the 10^{-10}Torr-range. Since hydrogen is the working gas in fusion devices, the high-temperature bake is usually not required in metal vessels used in fusion applications. For graphite walls, on the other hand, there is considerable evidence that baking to about 350 °C is the first necessary step toward achieving optimum wall conditions. This is the temperature necessary to drive out the water molecules located in the graphite pores in quantities up to ~1Torr-L/g. Therefore, using significant amounts of graphite in the plasma vessel, usually requires high-temperature baking. If non-graphite plasma-facing components can be utilized for the device, baking requirements are relaxed and the lower baking temperatures can substantially reduce the engineering requirements of the device. Choices for materials of PFCs will be discussed below.

10.2.3. Glow Discharge Cleaning

Glow-Discharge Cleaning (GDC) is today's standard wall conditioning technique for fusion devices. Most experiments use two or more fixed GDC anodes. GDC can be carried out in hydrogen isotopes for chemical clean-up of oxygen etc. or for wall pre-loading with specific hydrogen isotopes, or it can be performed in helium which provides physical cleaning by

sputtering and hydrogen removal by particle-induced desorption. Given uncertainties about GDC initiation and performance in the QPS geometry, the Helium Glow Discharge Cleaning (HeGDC) equipment should be designed for 2 ports with 4.5 inch O.D. flanges equally spaced toroidally for fixed wall anodes. These anodes will be used for both GDC and gaseous boronization. To reduce the pressure during the GDC, pre-ionization filaments or rf-assisted glow will be used, if necessary. This reduces the working pressure to values of $\leq 10^{-3}$ Torr, which is easier to handle by the turbo-pumps for long duration pumping.

10.2.4. Boronization

Boronization is a much desired wall conditioning technique, because it has led to improved performance in every single fusion machine to which it was applied. Boronization dramatically reduces the oxygen content of the plasma by gettering and provides low-recycling walls. The QPS boronization method should be sufficiently convenient and economical to be an operational tool that can be applied quickly and as often as required. It should also have minimal environmental, health, and safety impact. It should be possible to use hydrogenated or deuterated boron compounds depending on subsequent plasma operations.

A suitable and comparably effective candidate compound for QPS boronization is Trimethylboron [$B(CH_3)_3$ or $B(CD_3)_3$] which is presently in use on many fusion devices. Trimethylboron (TMB) is about a 1000 times less toxic than diborane and nonexplosive. TMB boronization was first tested on TEXTOR where it was found to be comparable in effectiveness to Diborane and considerably safer [15].

For the standard boronization procedure we follow a prescription used by Kugel on NSTX [16]. Specific safety measures are applied, which have become standard operating procedures in many fusion devices of today. Power supplies of ~450V, ~1A per anode will be used. A mixture of 90% He and 10% TMB [$B(CH_3)_3$ or $B(CD_3)_3$] is injected into the HeGDC until the TMB is consumed. This application is followed by HeGDC to remove the co-deposited hydrogen or deuterium from B/C film [16].

10.3. Plasma-facing Components and Divertor Configuration

10.3.1. Limiter vs. Divertor Operation

The difference between divertor and limiter operation is often not very obvious, therefore it is useful to define the main characteristics of the two modes of operation as we will use them in this proposal:

1. <u>Divertor</u> plates intercept open field lines. This could be islands or stochastic regions outside the separatrix. Hence, divertor plates have some edge plasma as buffer between the solid surface and the confined core plasma. This is advantageous for neutrals re-ionization and high recycling operation as well as for impurity screening. For symmetric operation in a stellarator, one set of divertor plates for each field period is needed.

2. Limiters intercept closed field lines of the confined core plasma. Here, the connection lengths are long (at least several toroidal revolutions), and the solid limiter surface is in direct contact with the confined plasma. The limiter acts as a major recycling source of neutrals as well as a major impurity source released into the main plasma. But, on the other hand, the limiter provides a well-defined plasma edge and may prevent uncontrolled plasma-interactions of islands or stochastic regions at certain parts of the wall.

Limiter operation might be the best way to start operation of QPS, while in later stages the advantages of a separatrix should be fully utilized by having any solid surfaces remote from the main plasma, controlling neutrals and possibly impurities by divertor baffles.

10.3.2. Magnetic Topology Outside the LCMS and Divertor Configuration

First results on field-line tracing outside the last closed magnetic surface in QPS show that the connection lengths of field-lines launched within a few cm outside the LCMS are long (several toroidal revolutions). This looks favorable for effective power and particle control with PFCs located outside the LCMS, i.e. in divertor configuration.

To determine where power and particles leave the confined plasma, i.e. as guidance for the design of the plasma-facing components, we have started to generate field-line plots outside the LCMS for the top, inside and outside of the cross-sections at the start and halfway through the field–period. First results of Poincaré plots, with an example in Fig. 10.1, indicate that the areas of most pronounced island formation and strongest clustering of field line punctuations are in the top and bottom of the bean-shaped cross-sections ($\phi = 0$). In the particular plot shown in Fig. 10.1, a total number of 30 field lines were launched, starting at the outboard midplane separatrix, 2 mm apart from each other. These field lines were followed many revolutions, until they intercepted a conformal surface at 10 cm from the LCMS, where they were stopped. The plot clearly indicates island formation outside the LCMS, in particular at the top and bottom of the cross-section. These are the areas where the interception of the boundary energy- and particle flows will be most efficient. Approximate shape and positions of top and bottom divertor baffles are indicated. It is clear, of course, that the baffles have 3-D configurations and change their shape as a function of toroidal angle ϕ.

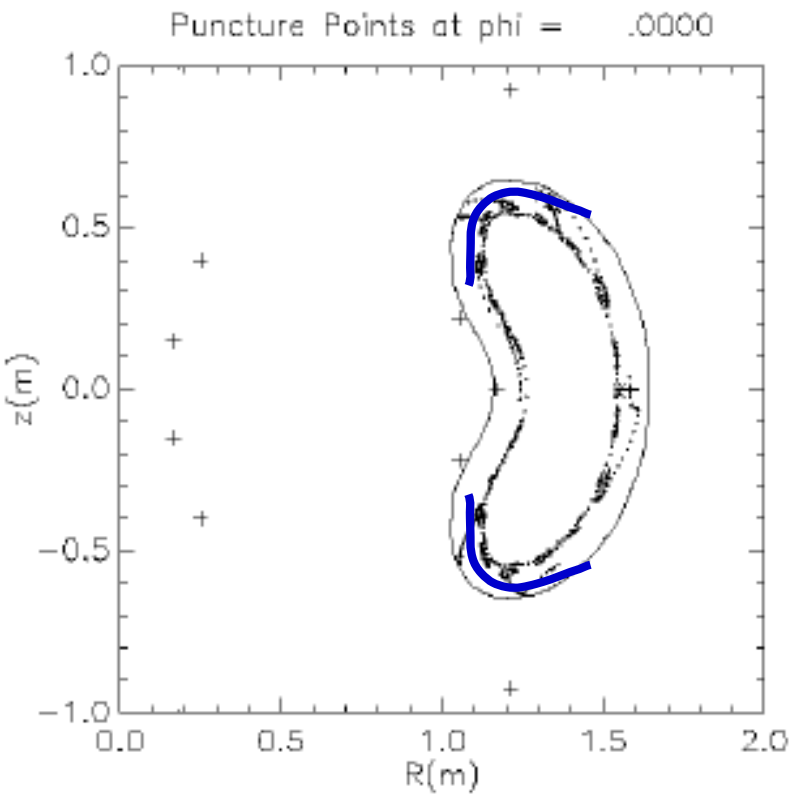

Fig. 10.1 Puncture plots of 30 field lines launched at the outer midplane separatrix, 2 mm apart; outer black contour: 10-cm conformal surface; blue objects: schematic divertor baffles.

The three-dimensional view of the divertor baffles (gray) along with the plasma surface (red) is depicted in Figure 10.2. The figure shows a schematic view of the divertor baffles; the exact shape and location, i.e. poloidal and toroidal extend, will be optimized with the aid of neutrals modeling.

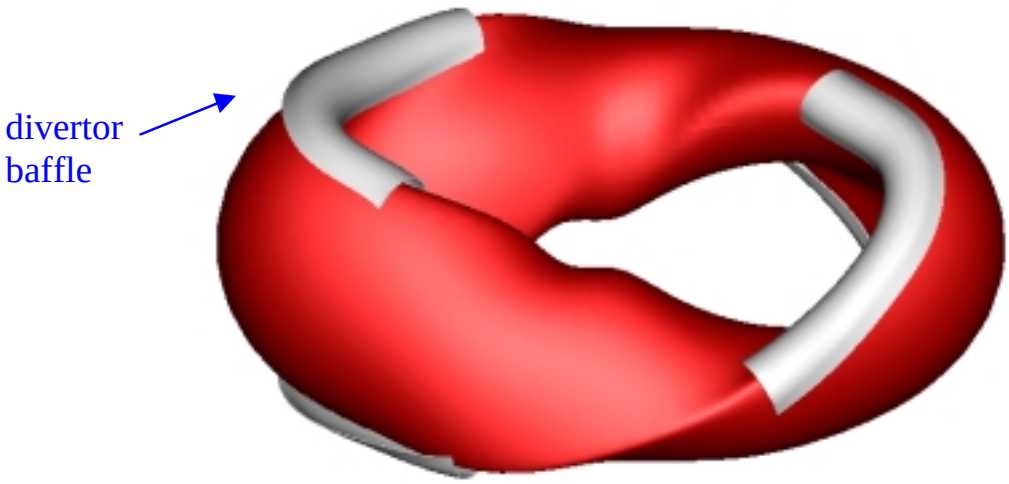

Figure 10.2 The QPS plasma surface (red) and the divertor baffles (2 per field-period) running along the helical edge of the plasma

10.3.3. Power and Particle Handling

Power and particle handling is to a large extend determined by design and material of the plasma-facing components (PFCs). The PFCs are typically designed for handling up to 80% of the total input power and, ideally, to provide some neutrals control.

As discussed above, the materials choice for the PFCs also has a strong impact on the baking temperature and, therefore, on the engineering of the device. For our baseline design, we consider the use of locally in-situ bakeable graphite or boron carbide for the PFCs. Boron carbide has the advantage of having a low atomic number Z with some promise not to need the high-temperature bake-out like graphite. It's main weakness in comparison with graphite is the lower thermal shock resistance. But for the power fluxes anticipated in QPS, this shouldn't present a problem. Boron carbide has been tested for limiter applications and showed thermal shock fracture under conditions of 24 MW/m^2 for t = 0.5s [17]. The PFCs for QPS will be designed in a way so that the power flux does not exceed 10 MW/m^2 for 0.5 s. The actual materials choice and necessary bake-out temperatures have yet to be finalized.

The total heating power in QPS will be 1.4 MW: 0.4 MW of ECH and 1.0 MW of ICRF and the pulse duration will be $\leq$ 1 s, realistically not above 0.5 s. With a given input power, the necessary surface area of the divertor plate is determined by the maximum allowable surface temperature. If we specify a maximum allowable power flux of 10 MW/m^2 for 0.5 s, a surface area of 0.14 m^2 would be necessary under the assumption of uniform power deposition. However, since we don't know the distribution of the power flux at this point, we need to specify a peaking factor (or an area factor) to design for safe power handling. Peaking factors of 3 are common in designing PFCs if some experience is available, but since we are very uncertain about the QPS boundary at this stage, we assume a peaking factor of 5 to be on the safe side. This means that we need a surface area of 0.7 m^2.

To estimate the area of the divertor baffle, we can measure the poloidal length of the divertor baffles from Figure 10.2 to be about 0.5 m. Assuming that each baffle covers about 60 degrees toroidally, then the total toroidal length would be 2/3 of the toroidal circumference, or about 4 m. This would result in a total divertor baffle area of 2 m^2, i.e. the total available surface area is more than sufficient to handle the power and stay well below the limits of boron carbide. The main question remains, of course, how the power flux in the edge is distributed, i.e. what peaking factors result due to islands and other features in the boundary topology.

Particle and impurity control play a key role in optimizing plasma performance. Impurity control starts with the materials choice and the proper design of the PFCs. Proper design includes, e.g. that the field lines intercept the PFC surfaces at shallow angles to spread out the heat flux as much as possible and prevent excessive power flux densities and surface temperatures. To provide the magnetic topology for the PFC design, we will study the magnetic field configuration outside the LCMS in detail. Detailed power flux estimates will

be performed by using field-line-following codes to generate foot prints on the divertor baffles and estimate the area "wetted" by the plasma.

Control of neutrals has been shown to improve plasma performance, from the first H-mode observation resulting from closely fitting divertor baffles [2] to the control of recycling by wall conditioning with pumping surfaces [1]. In QPS the effort to control neutrals will consist of several components: the first element of control is given by the PFCs which will be shaped and positioned so as to minimize the neutral density outside the confined plasma, the second means of control will be given by wall conditioning with hydrogen-pumping films as created by boronization, and the third way of reducing neutral densities will be provided by large-area getter panels in the top of the bell-jar. While the wall conditioning and large-area getter panels are means of reducing the neutrals density in the bell-jar overall, the PFC design will be more specific and will be guided by plasma boundary neutrals transport codes such as DEGAS [19]. Finally, the gas puff nozzle will be positioned at a coil location close to the plasma to enhance direct fueling of the plasma rather than filling of the bell-jar with neutral gas.

10.4 Operation with Pre-Cooled Coils

The coil temperature range from the beginning to the end of the pulse is a crucial parameter for the necessary coil size as well as the pulse duration. Details are discussed in section 3.6. Since under the present design option the coils are located inside the vacuum vessel, the coil temperature can potentially become an impurity control issue. If the temperature of the coil casings is below ambient temperature, the concern is that impurities in the residual gas will accumulate on the cooler surfaces between shots and then be released under plasma bombardment during the subsequent discharge.

To estimate the effect of cooler surfaces within the bell-jar, we calculate the impurity surface coverage on the cooler surfaces. The difficulty is that surface physics effects are usually studied under “clean” conditions, i.e. on super-clean single crystal surfaces with well defined conditions such as adsorption energies, etc. However, technical surfaces deviate grossly from these ideal surfaces by having various degrees of surface roughness, oxide layers, contaminants, and ill-defined adsorption energies, sticking coefficients, etc. Hence, quantitative estimates have to be taken with a grain of salt, but still should give us a rough idea of the effects of impurity accumulation at cooler surfaces.

In the following, we discuss the basic adsorption/desorption considerations for impurity accumulation. The controlling parameter is the time for which an adsorbed particle stays on the adsorbing surface, the “time of sojourn” τ , which is given by the Frenkel equation [18]:

$$\tau(T) = \tau_0 \exp(E_D/RT),$$

with $\tau_0 = 10^{-13}$ s the period of vibration of the particle on the surface, E_D [kJ/mole] the activation energy for desorption, R = 8.314 [J/K.mole] the gas constant, and T [K] the absolute temperature. As an example, the results are shown in Figure 10.3 for the surface

adsorption of O_2 on stainless steel, with an adsorption energy of 71 kJ/mole and for the temperature range of 270 K to 350 K. Assuming an ambient temperature of 300 K and a coil casing temperature of 273 K, i.e. a temperature difference of only 27 degrees, Figure 10.3 shows a factor of about 16 in the time of sojourn for this relatively small temperature difference.

Other relevant residual gases are O_2, N_2, CO, CO_2, and C_3H_8 which all have desorption energies in the range of 66 to 74 kJ/mole; the only gas with significantly higher desorption energy on stainless steel is H_2O with about 94 kJ/mole. Methane, CH_4 has much lower desorption energies in the range of 50 kJ/mole. For water molecules with about 30% higher desorption energies than oxygen, the difference in sojourn time is a factor of 41.

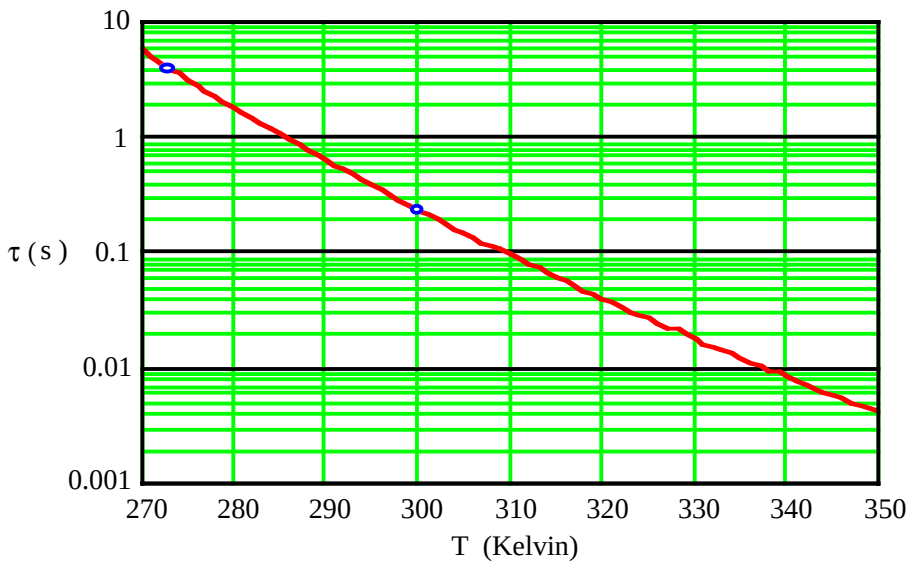

Figure 10.3. Time of sojourn of O_2 molecules adsorbed on stainless steel, as a function of surface temperature: τ = 4 s at T = 273 K and τ = 0.24 s at T = 300 K..

So, due to the exponential dependence, relatively small differences in substrate temperatures can lead to fairly large differences in the sojourn time of the relevant species on the surface.

In equilibrium, the amount of gas on the surface is determined by the balance between the rates of adsorption and desorption. The rate of adsorption R_A is given by

$$R_A = \alpha \frac{n\,v}{4} = \alpha \cdot 3.5 \cdot 10^{22} \frac{p}{\sqrt{M \cdot T_G}}, \qquad (1)$$

with α=0...1 the sticking coefficient, n and v the density and mean velocity of the gas molecules, p the gas pressure, M the molecular weight, and T the gas temperature in Kelvin. The sticking coefficient can vary strongly with the surface conditions and we take here a typical value of α = 0.1.

The rate of desorption R_D is given by:

$$R_D = \frac{N}{\tau} = \frac{N}{\tau_0}\, e^{\frac{-E_D}{R \cdot T}} \qquad (2)$$

where N is the surface coverage on the substrate in particles per unit area.

In equilibrium, we have $R_A = R_D$ and the surface coverage as a function of temperature is:

$$N(T) = \left(\alpha \cdot 3.5 \cdot 10^{22}\, \frac{p}{\sqrt{M \cdot T_G}}\right) \tau_0\, e^{\frac{E_D}{R \cdot T}}. \qquad (3)$$

The equilibrium surface coverage in particles per cm^2 is then, with $\alpha = 0.1$ and M = 16, the gas temperature $T_G = 300$ K, $p = 5 \times 10^{-9}$ Torr: for T = 273 K, $N = 1 \times 10^{12}$ cm^{-2} and for T = 300 K, $N = 6 \times 10^{10}$ cm^{-2} . Figure 10.4 shows the equilibrium surface coverage for the temperature range of 270 to 350 K.

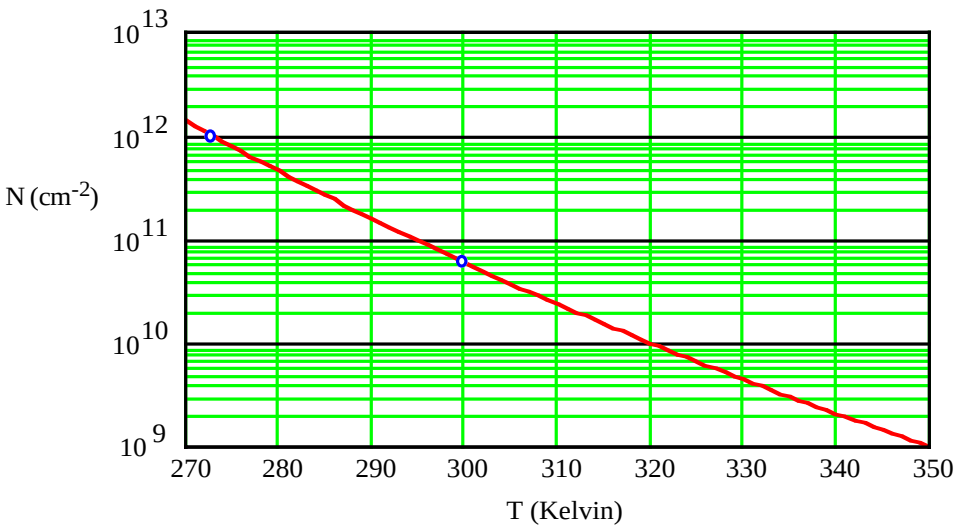

Figure 10.4 Equilibrium surface coverage N (particles per cm^2) for particles with 71 kJ/mole desorption energy as a function of substrate temperature T.

Since we have not changed the sticking coefficient or any other parameter as a function of temperature, the surface coverage shown in Figure 10.4 reflects essentially the sojourn time. By equating equations (1) and (2), we obtain the equilibrium surface coverage, but we don't know anything about the time in which the equilibrium is reached. So, in order to investigate if the equilibrium coverage is even reached between shots, we need to calculate the evolution dN/dt of the coverage:

$$\frac{dN}{dt} = \alpha \cdot 3.5 \cdot 10^{22} \cdot \frac{p}{\sqrt{M \cdot T}} - \frac{N}{\tau_0}\, e^{\frac{-E_D}{R\,T}} . \qquad (4)$$

The solution of this differential equation for T = 273 K and for T = 300 K is depicted in Figures 10.5a and 10.5b.

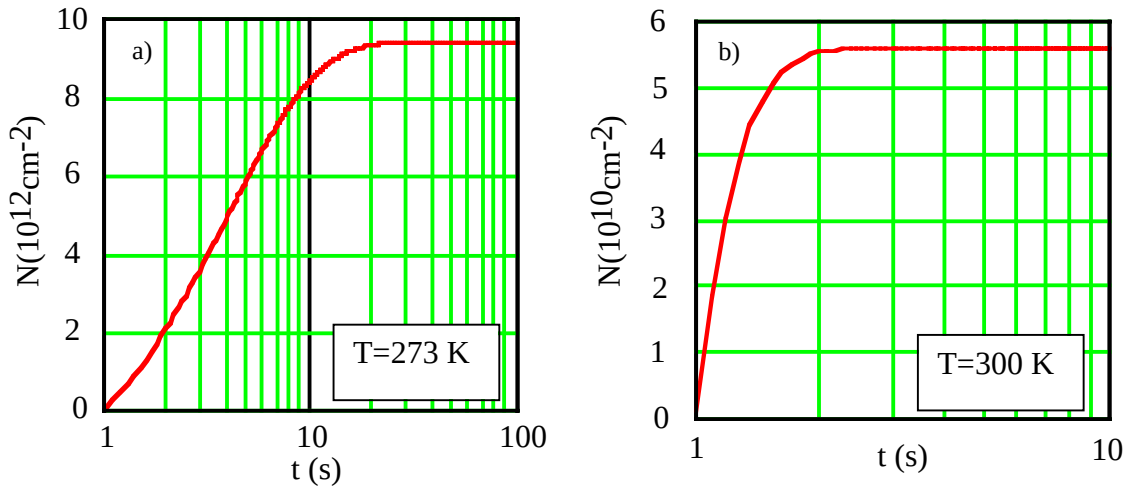

Figure 10.5a Evolution of surface coverage for substrate temperature of 273 K and 10.5b evolution of surface coverage for substrate temperature of 300 K.

As expected, at lower temperature the desorption rate is slowed down and it takes a larger number of adsorbed particles to reach equilibrium, i.e a longer time to reach equilibrium. But in either case, the time to reach equilibrium is short in comparison with the expected time between shots which is likely to be in the range of 600 s. In other words, all species with low desorption energies, around 70 kJ/mole or lower, will reach equilibrium coverage between shots.

Since the surface coverage increases exponentially with the activation energy for desorption, increased desorption energies will quickly lead to higher surface coverages. Water molecules with 94 kJ/mole can build up significant fractions of a monolayer (i.e. ~5 x $10^{18}m^{-2}$) within the nominal 600 s exposure time between discharges.

<u>Conclusions</u>. The above discussion on adsorption/desorption leads to separate conclusions for species with low and higher binding energies. First, we look at low desorption energies up to 71 kJ/mole; if the total low-temperature surface area is as large as the vacuum vessel and roughly 1/4 of it is exposed to the plasma, then the total number of impurities accumulated here and available for the plasma is: N_i = (9 x 10^{11} cm^2) x (10^4 cm^2) x (15 m^2) = 1.35 10^{17} particles. This would be less than one percent of the plasma inventory. This seems to be manageable, although not desirable, because we have to keep in mind, that major uncertainties in the estimates are in the sticking coefficients and in the desorption energies, both of which depend strongly on the surface conditions.

The situation for species with higher desorption energies appears to be quite different. Within about 600 s between shots, desorption of these species remains low due to the high surface

binding energy. For the assumed partial pressure of 5 x 10^{-9} Torr and a sticking coefficient of 0.1, significant fractions of a monolayer can be accumulated. This would clearly be a sufficient number of impurity particles to contaminate the plasma significantly; so, this situation needs to be avoided. A possibility to remedy the surface build-up of impurities would be to apply surface coatings such as boronization which should lower the sticking coefficients as well as the surface binding energies thus lowering adsorption and increasing desorption. But this would be a fix for the case that all else fails and is not a recommendable strategy. Overall, this analysis indicates that the existence of surface areas with lower than ambient temperatures in the vacuum vessel, even if the temperature difference is only between 273 and 300 K, should be avoided if at all possible.

10.5. Initial Experimental Plasma Boundary Program

Initially, it will be most important to analyze the boundary topology and measure the most significant plasma parameters, using basic edge diagnostics. Once we have a first experimental picture of the plasma boundary, we will be able to design more advanced diagnostics and determine the optimum locations within the 3-dimensional boundary. At this stage, we will study the plasma boundary in order to optimize the plasma-wall interactions in support of improved plasma performance of QPS.

Magnetic Boundary Topology:

Since the topology of the plasma boundary is 3-dimensional and complex, with ergodic regions and island areas and probably also well-ordered laminar areas near the coils, flux surface mapping is the first experimental task to be accomplished in the edge plasma program. Usually, this is done in vacuum and, accordingly, yields the vacuum flux surfaces. The applied technique consists of a radially moveable electron gun and a fluorescent mesh. The flux surfaces are obtained by taking pictures of the electron beam intercepted by the fluorescent mesh while changing the radial position of the electron gun. The flux surface images are taken with a tangential view of a charge-coupled device (CCD) camera. This method of mapping the flux surfaces has been applied to about all of today's stellarators, from ATF to LHD [19].

Power- and Particle Control:

In the area of power- and particle handling, measuring the global power balance will be among the first tasks. This is important because 1) we need to know through which channels the plasma energy is lost and 2) it is necessary to monitor the power flux to the plasma-facing components to ensure that they don't get excessively hot. The balance between input power, radiation, convection and conduction to the plasma-facing components will initially be measured with a bolometer array, infrared-sensitive cameras and instrumented wall components such as divertor baffles.

In the area of particle control, the most important technique will be wall conditioning, as described above. In addition, recycling control by well-positioned neutrals baffles will

contribute to keep the neutrals concentrated in the areas where they are born. The main diagnostics to investigate recycling patterns will be H-alpha arrays viewing the divertor baffle areas and the "skinny" cross-section of the bean shape.

For the initial operation, we will also have a survey spectrometer which will be used to determine the main plasma impurities and also to determine causes and remedies of possible thermal collapses by radiation, which often occur during initial plasma operation.

Edge Plasma Parameters:

The initial set of edge plasma diagnostics will consist of filter-scope arrays to monitor H-alpha and impurity lines, a survey spectrometer, Langmuir probes, cameras for infrared and visible light, a bolometer, and instrumented divertor baffles. With this set, we will be able to measure the basic edge parameters such as density, temperature, particle fluxes, heat fluxes, and major impurity radiation. Since the edge plasma is 3-dimensional and non-uniform, it will be important to probe the overall topology and characteristic features of the boundary. To be able to do this, larger areas of the edge need to be diagnosed to determine the location of the features to be investigated. This will be accomplished with a combination of imaging techniques (cameras), scanning probes, and modeling of the edge.

Optimization of Plasma-Wall Interactions:

At a later stage, the goal of the plasma edge program will be to determine the best combination of power- and particle-intercepting baffles with most effective wall conditioning techniques. Designing the divertor baffles so as to spread out the power flux as much as possible and simultaneously controlling the neutrals where they are generated, which is most likely in the top and bottom of the bean-shaped cross-sections. Optimization of the divertor baffles for neutrals control will accomplished with the help of neutrals transport codes such as DEGAS [20], a technique we have successfully applied to tokamaks in the past [21].

References:

[1] J. Winter, Plasma Phys. Control. Fusion 38 (1996) 1503

[2] F. Wagner et al., Phys. Rev. Lett. 49, 1408 (1982)

[3] G. Jackson et al., Phys. Fluids B 4 (7), July 1992

[4] R. Grigull et al., J. Nucl. Mater. 196-198 (1992) 101

[5] A. Sagara et al., J. Nucl. Mater. 241-243 (1997) 972

[6] B. Carreras et al., Phys. Plasmas, Vol. 5, No.7 (1998) 2623

[7] R. Colchin et al., Nucl. Fusion, Vol.40, No.2 (2000) 175

[8] H. F. Dylla et al., J. Nucl. Mater. 162-164 (1989) 128

[9] A. M. Messiaen et al., Phys. Rev. Lett.,Vol.77, No.2 (1996) 2487

[10] M. Murakami et al., Nucl. Fusion, 41 (2001) 317

[11] L. A. Berry et al., Plasma Phys. and Contr. Fusion, Vol.1, IAEA, Vienna (1975) 101

[12] R. J. Elsey, Vacuum, Vol. 25, No 8 (347) 1975

[13] Outgassing Data Sheets, P. Goranson, private communication

[14] L.A. Berry, private communication
[15] J. Winter, et. al. J. Nucl. Mater. 176 &177 (1990) 486
[16] H. W. Kugel, et al., Bull. Am. Phys. Soc. 45 (7), 251 (2000).
[17] M. Ulrickson, J. Nucl. Mater. 85&86 (1979) 231
[18] J. Frenkel, Zeit. fur Phys. 26 (1924) 117
[19] R. J. Colchin et al., Rev. Sci. Instrum. 60 (1989) 2680
[20] D. B. Heifetz et al., J. Comput. Phys. 46 (1982) 309
[21] P. K. Mioduszewski et al., J. Nucl. Mater., 176&177 (1990) 733